Thickness-Dependent Magnetotransport Properties in 1T VSe_2 Single Crystals Prepared by Chemical Vapor Deposition

Yunzhou Xue, Yi Zhang, Huichao Wang, Shenghuang Lin, Yanyong Li, Ji-Yan Dai, Shu Ping Lau*

Department of Applied Physics, The Hong Kong Polytechnic University, Hung Hom, Kowloon, Hong Kong, P. R. China

*Corresponding author E-Mail: apsplau@polyu.edu.hk

ABSTRACT

Two-dimensional (2D) metallic transition metal dichalcogenides (TMDs) exhibit fascinating quantum effects, such as charge-density-wave (CDW) and weak antilocalization (WAL) effect. Herein, low temperature synthesis of 1T phase VSe_2 single crystals with thickness ranging from 3 to 41 nm by chemical vapor deposition (CVD) is reported. The VSe_2 shows a decreasing phase transition temperature of the CDW when the thickness is decreased. Moreover, low-temperature magnetotransport measurements demonstrate a linear positive and non-saturating magnetoresistance (MR) of 35% from a 35-nm-thick VSe_2 at 15 T and 2 K due to CDW induce mobility fluctuations. Surprisingly, Kohler's rule analysis of the MR reveals the non-applicability of Kohler's rule for temperature above 50 K indicating that the MR behavior cannot be described in terms of semiclassical transport on a single Fermi surface with a single scattering time. Furthermore, WAL effect is observed in the 4.2-nm-thick VSe_2 at low magnetic fields at 2 K, revealing the contribution of the quantum interference effect at the 2D limit. The phase coherence length $l_{\emptyset}$ and spin-orbit scattering length l_{so} were determined to be 73 nm and 18 nm at 2 K, respectively. Our work opens new avenues to study the fundamental quantum phenomena in CVD-deposited TMDs.

Keywords: Vanadium Diselenide, Chemical Vapor Deposition, Charge Density Wave, Magnetoresistance, Weak Antilocalization

Transition metal dichalcogenides (TMDs) are a class of layered materials with variety of physical properties ranging from semiconducting to metallic. Specifically, two-dimensional (2D) metallic TMDs host a cornucopia of exotic physical phenomena such as superconductivity [1-5], ferromagnetism [6-10] and charge density waves (CDWs) [11-17], which are dramatically distinguished with their bulk states, resulting in worldwide attention. The three-dimensional Fermi surface nesting (3D-FSN) [18], electron-phonon coupling (EPC) [19, 20] and saddle-point singularity [21, 22] were proposed to explain the CDW phenomenon in different materials. Nowadays, the concept of CDW has already widely permeated into some of the metallic TMDs [21, 23]. Among all the metallic TMDs with CDW, VSe_2 has attracted special interest. VSe_2 is a typical layered metallic material with 1T octahedral structure. The V atoms are sandwiched between two layers of Se atoms to form a single molecular layer. The individual VSe_2 layers are coupled by weak van der Waals interaction without lateral displacement as shown in Figures1a and b. It shows $4a \times 4a \times 3a$ wavelength for its CDW in the bulk at phase transition temperature (T_P) of 110 K [24, 25]. However, for ultrathin VSe_2 flakes, their T_p values are controversial. Xu *et al*. and Pásztor *et al*. reported that the T_p increased (122 - 135 K) when the samples thinner than 10 nm [8, 26], but Zhang *et al*. claimed that the T_p reduced (60 - 72 K) [16]. These discrepancies may be related to the crystal quality of the sample, substrate effect and preparation method.

New phenomena in layered TMDs have been discovered continuously. The resistance of the materials respond to the external magnetic field, results in the increasing of electrical resistance, namely magnetoresistance (MR). The MR is the fundamental physics phenomenon of the interactions between electrons and the magnetic field. Recently, WTe_2 has found to exhibit the largest known non-saturating MR in the bulk

due to the perfect compensation of electron and hole bands [27] and the weak antilocalization (WAL) in the ultrathin form [28]. One of the attractive features of WAL is that it can facilitate the investigation in the interacting magnetic systems, such as Kondo impurities, spin fluctuations, and valence mixing [29]. However, WAL effects are rarely reported in TMDs especially in light transition metal dichalcogenides [30].

Herein, we report low temperature (~350 °C) synthesis of 1T VSe_2 single crystals on sapphire substrate by CVD method. The VSe_2 crystals were grown vertically on the sapphire surface, which facilitates easy transfer to any other substrates by simply pressing the as-grown sample onto the new substrates. The direct transfer method could ensure the quality of the samples and minimize the contaminants due to chemical/physical transfer processes. For our VSe_2 crystals, the transition temperature T_p decreases when the crystal thickness is decreased from 35 nm to 4.2 nm. Most importantly, the 35-nm thick VSe_2 exhibits a positive and non-saturating MR of ~35% at 15 T and 2 K. Besides, WAL effect can be observed at low fields in the 4.2-nm-thick VSe_2, illustrating the quantum interference effect at the 2D limit.

RESULTS AND DISSCUSSION

Figure 1c shows the schematic diagram of the VSe_2 growth. In brief, VCl_3 and Se were used as the precursors at the growth temperature of 350 - 400 °C under ambient pressure. The sapphire substrate was placed at the center of the furnace with the polished side faced up. The VCl_3 and Se powder were placed upstream 6 - 7 cm and 4 - 5 cm away respectively from the sapphire substrate. A 10% H_2/Ar mixture gas was used as the carrier gas. Figure 1d and Supplementary Figure S1 show the scanning electron microscopy (SEM) images of the standing VSe_2 crystals on the substrate. The standing

crystals usually have the longest edges bonded to the substrate. The dangling bonds on the sapphire surface [31], the mismatching surface energies between VSe_2 and the substrate [32] may facilitate the vertical grown of the VSe_2.

X-ray photoelectron spectroscopy (XPS) was performed to detect the chemical composition of the VSe_2 crystals (Figure 1e). The Se 3d peak located at 54.3 eV can be considered as Se^{2-}, and both of V $2p_{3/2}$ and V $2p_{1/2}$ peaks located at 513.5 eV and 521 eV can be ascribed to V^{4+}.[16] As is known, the 1T VSe_2 structure is trigonal D_{3d}^3 and each unit cell contains one formula unit. To identify the phase structure, Raman spectroscopy was employed. The A_{1g} and E_g modes of 1T VSe_2 are located at 206 cm^{-1} and 136 cm^{-1}, respectively, and the E_g mode is weak and broad as shown in Figure 1f. No oxidation-related peak can be observed at around 252 cm^{-1}, indicating its high crystal quality. In contrast to other 2D TMDs, the A_{1g} and E_g modes of the VSe_2 remain unchanged with thickness ranging from 3 to 40 nm as shown in Supplementary Figure S3a. Atomic force microscopy (AFM) was used to determine the thickness of the VSe_2 crystals. The representative AFM images are displayed in Figures 1g and Supplementary Figure S4. The thickness of the VSe_2 crystals varies from 3 nm to about 41 nm.

The microstructure of the VSe_2 can be identified from the atomic-resolution high-angle annular dark-field scanning transmission electron microscopy (HAADF-STEM) images. Due to the Z-contrast of HAADF-STEM image, as shown in Figure 1h, the Se columns have a higher intensity than the V columns, which are marked with red and blue circles, respectively. Figure 1i shows the enlarged false colour image indicated by the rectangular box in Figure 1h and the elemental contrasts can be clearly seen. As shown in Figure 1j, the intensity profile taken along the yellow line in Figure 1i further demonstrates the positions of V and Se atoms. We note that each V atom is surrounded

by six Se atoms and the adjacent layers aligned in the vertical direction to form well defined atomic columns, which are consistent with the projection model of 1T phase VSe_2 (Figures 1a and b).

A CDW always accompanies with an anomaly in the resistivity, specifically, the resistivity increases with decreasing temperature in certain temperature range. Six-terminal Hall bar devices (inset in Figure 2a) were fabricated to study the temperature-dependent resistivity of the VSe_2 crystals, namely, to determine the T_p. Figure 2a presents the resistivity normalized at 300 K versus temperature (R-T curves) for VSe_2 with thickness ranging from 4.2 nm to 35 nm. When the temperature decreases, the resistance decreases. An upturn kink emerges at temperatures below 100 K for VSe_2 with various thicknesses. The resistance anomalies are attributed to the CDW transition as the transition depletes density of states on part of the Fermi surface [33, 34]. For the temperature between 100 K and 300 K, the resistivity exhibits a linear relationship with temperature, indicating the dominant electron-phonon scattering mechanism within this range. Figure 2b shows the first derivative (dR/dT) of the R-T curves. The T_p is defined at its minimum point of the dR/dT [13]. Figure 2c shows the T_P as a function of the thickness. As the thickness reduces from 35 nm to 4.2 nm, the T_p monotonically decreases from 100 K to 62 K, indicating that the CDW order in the VSe_2 is suppressed as compared to their bulk counterparts. The monotonic thickness dependence of T_p below 10 nm is consistent with the transport results of the mechanically exfoliated [13] and CVD-deposited VSe_2 [16], but contrary to the scanning tunneling microscopy results of ultrathin VSe_2 [26]. This inconsistence may be related to the crystal quality of the sample, substrate effect as well as sample preparation method.

The residual-resistivity ratio ($R_{300\,K}/R_{5\,K}$, RRR) serves as an indication of the purity and overall quality of a crystal. Figure 2d shows the RRR of the VSe_2 as a function of

thickness. The highest RRR value can reach up to 18.5 for the 35 nm thick VSe_2 sample, which is much higher than other works (Figure 2d). However, the RRR value decreases from 18.5 to 2.7 as the thickness decreases from 35 nm to 4.2 nm. This phenomenon is attributed to the enhanced disorder effect in the thinner VSe_2 after the transfer and device fabrication processes [13]. The electrical conductivity of VSe_2 (35 nm) is around 10^6 Sm^{-1} at 300 K and further increases to 1.53×10^7 Sm^{-1} at 2 K as shown in Supplementary Figure S6, which are also higher than the reported values (~3.4 x 10^6 Sm^{-1} at 2K) [16]. The T_p of the VSe_2 samples were found to be independent of the cooling and heating process as well as the magnetic field strength (up to 15 T) as shown in Supplementary Figure S7f and Figure S8, respectively. Figures 2e and f show the resistivity-dependent of magnetic field as a function of sample thickness and temperature, respectively. The sign of Hall resistivity indicates n-type conduction. The Hall resistivity decreases as the field increases and reveals a linear relationship. It should be noted that no anomalous Hall effect signal could be observed, suggesting that the VSe_2 exhibits no intrinsic ferromagnetism even the thickness is down to 4.2 nm.

In conventional metals, the trajectory of an electron can be bended by the Lorenz force induced by a magnetic field. In turn, the movement of the electrons will be affected under the action of electric field, results in the increasing of electrical resistance. The increase of the resistance with the applied magnetic field usually leads to positive MR and it tends to saturate at high fields [35]. However, non-saturating linear MR also can be obtained in some special materials, such as Bi_2Te_3 [36], $Ag_{2+\delta}Se$ and $Ag_{2+\delta}Te$ [37]. Figure 3a shows the MR of the VSe_2 with various thicknesses at 2 K. The out-of-plane magnetic field of up to 15 T was applied. The VSe_2 samples exhibit the quadratic magnetic field dependence at the low field but linear MR at high field. It shows non-saturating MR even at 15 T. The linear MR may originate from CDW induce mobility

fluctuations [30], rather than from quantum mechanism, as no Shubnikov-de Haas oscillation is observed at high magnetic field [38]. The MR increases as the thickness of the VSe_2 increases, and the highest MR can reach up to 35% for the 35-nm-thick VSe_2 (Figure 3a), which is 1 to 2 orders of magnitude higher than that of the bulk VSe_2 [39, 40]. Figure 3b shows the MR of the VSe_2 (35 nm) at different temperatures. It demonstrates that the MR increases as the temperature decreases from 150 K to 2 K. In order to investigate the relationship between the MR and carrier mobility (Supplementary Information), the temperature dependent MR of the 35-nm-thick sample at 15 T were measured and the corresponding extracted carrier mobility curve are shown in Figure 3c. The behavior in the range from 2 K to 300 K indicates that the non-saturating linear MR of the VSe_2 is likely attributed to the carrier fluctuation [41]. The consistent trends of MR and the mobilities for different thicknesses further support this mechanism as shown in Figure 3d.

We also examined the applicability of Kohler's rule in the VSe_2 system. In the conventional metallic material, it only has a single species of charge carrier and the scattering time (τ) is the same at all points. It does not depend significantly on the location along the Fermi surface. Thus, the MR obeys the general function known as Kohler's rule and is expected to collapse into a single curve measured at different temperatures [41]. The Kohler's rule is given as

$$\frac{\rho(H,T)-\rho(0,T)}{\rho(0,T)} = F(\omega_C\tau) = f\left(\frac{H}{\rho(0,T)}\right) \quad (1)$$

where H is the magnetic field, T is the temperature, ρ(H,T) is the magnetic field resistivity, ρ(0,T) is the zero-field resistivity and ω_C is the frequency at which the magnetic field causes the charge carriers to sweep across the Fermi surface. The plot of $\frac{\rho(H,T)-\rho(0,T)}{\rho(0,T)}$ vs $\frac{H}{\rho(0,T)}$ are known as Kohler plot and as shown in Figure 3e. It is apparent that the curves at 2, 20 and 30 K collapse into a single curve (inset Figure 3e),

indicating that Kohler's rule is obeyed for VSe_2 below 50 K. However, it is clearly seen that the non-applicability of Kohler's rule for the curves at 50 K and 150 K, indicating that the MR behavior cannot be described in terms of semiclassical transport on a single Fermi surface with a single scattering time. The reasons of the observed transition from applicability to non-applicability of Kohler's rule with temperature increasing can be explained by the CDW induced pseudo gap opening in VSe_2. As mentioned above, CDW forms at about 100 K for ~35 nm thick VSe_2 samples. The formation of CDW leads to the gap opening and the reduction of carrier density [33]. The electron density drops can be clearly seen at around 100 K as shown in Figure 3f, indicating the pseudo gap opening of VSe_2 due to the formation of CDW, as it still keeps the metallic transport below T_p [33]. The partial gap opening has also been observed at M point in the first Brillouin zone by angle-resolved photoemission spectroscopy, while the Fermi surface at Γ point remains intact [34, 42]. Based on the above analysis, the applicability of Kohler's role below 50 K, indicates that one kind of carrier dominates the transport due to the CDW induced pseudo gap opening, which probably comes from the Fermi surface centered at Γ point. The contribution from the Fermi surface centered at M point is insignificant due to the pseudo gap forming here. At temperature above 50 K, Kohler's rule is violated, suggesting more than one type of carriers contribute to the transport because the CDW partial gap disappeared at high temperatue [43]. Carriers from the Fermi surface centered at M point probably contribute to another transport.

Figure 4a shows the magnetic field dependent MR of the 4.2-nm-thick VSe_2 sample. A sharp dip can be observed at low fields as marked by a red circle and the enlargement is shown in Figure 4b. Such a low field behavior is recognized as a signature of WAL effect, which originates from the interference of quantum coherent electronic waves

undergoing diffusive motion in the presence of spin-orbit interaction at low temperatures. Figures 4b and c present the WAL effects at low field under different temperatures, which are well matched with the fitting results of Hikami-Larkin-Nagaoka (HLN) theory (Supplementary Information) [28]. The magnitude of magnetoconductance decreases with the increasing temperature, as qualitatively expected for the WAL correction to the conductivity [28]. The dephasing fields $B_{\emptyset}$ can be extracted by fitting the magnetoconductance with HLN theory as a function of temperature, and keep B_{so} (the spin-orbit scattering field) constant due to its temperature independence. Through the fitting result we also can determine that the phase coherence length $l_{\emptyset}$ and spin-orbit scattering length l_{so} are 92 nm and 19 nm at 2 K, respectively. The l_{so} is comparable to the spin-orbit scattering length of 2H-$TaSe_2$ (~17 nm) [44], indicate the potential application of VSe_2 in 2D spintronics. As shown in Figure 4d, the linear temperature dependence of $B_{\emptyset}$ and the inverse square root temperature dependence of $l_{\emptyset}$ indicates that the electron-electron interactions are the dominant factor of dephasing in a diffusive system [28]. The observed WAL effect in the ultrathin VSe_2 crystal suggests that quantum interference effect is dominated at the 2D limit [45, 46]. It should be noted that only weak localization effect rather than WAL was observed in the mechanically exfoliated 2D VSe_2 and the observation was attributed to the defects [39]. Thus, the CVD-deposited 2D VSe_2 will open a new avenue to study the fundamental quantum phenomena in TMD materials.

CONCLUSION

In conclusion, the standing VSe_2 single crystals prepared by CVD method have provided a platform to study the CDW and magnetotransport properties of light-

transition-metal TMDs. The CDW phase transition temperature decreases from 100 K to 62 K with the thickness decreased from 35 to 4.2 nm and the highest RRR can reach up to 18.5, indicating its high crystal quality. A large linear positive and non-saturating MR of ~35% (at 15 T and 2 K) was obtained from the 35-nm-thick VSe_2. The non-applicability of Kohler's rule with temperature above 50 K and the abrupt changes of conductivity and carrier density can be explained by the CDW induced pseudo gap opening in VSe_2. The ultrathin VSe_2 demonstrates WAL effect at low fields. The linear temperature dependence of $B_\emptyset$ suggests the interactions between electrons are the origin of the phase relaxation. The phase coherence length $l_\emptyset$ and spin-orbit scattering length l_{so} are determined to be 73 nm and 18 nm at 2 K, respectively. Our work sheds light on the quantum interference effect of the VSe_2 at the 2D limit, which may spur further investigations.

METHODS

CVD growth of VSe_2 single crystals. The CVD growth process was carried out in a single heating zone furnace with 20 cm constant temperature zone and the inner diameter of the equipped quartz tube was 26 mm. Vanadium chloride (VCl_3) and selenium (Se) were used as the sources in the process of preparing VSe_2 crystals. VCl_3 (5 mg) and Se (1 g) powder in the quartz boats were put upstream 6 - 7 cm and 4 - 5 cm away from the furnace center, respectively. Sapphire substrate was put at the central part with the polished side faced up. Before heating, the furnace tube was evacuated with a rotary pump for 10 - 15 min and then filled with 10% H_2/Ar mixture gas to ambient pressure. After that, heating the furnace up to 350 - 400 °C with the heating rate of 20 °C /min and 110 sccm 10% H_2/Ar mixture gas was used as the carrier gas at the same time. The target temperature was kept for 10 - 20 mins. Then, the furnace was

rapidly cooled.

Characterization. The samples were systematically characterized by optical microscopy (Leica), SEM (TESCAN VEGA3), AFM (Bruker NanoScope 8), XPS (Kratos AXIS Supra/Ultra with monochromatic Al Kα X-ray), Raman spectroscopy (Witec_Confocal Raman system), XRD (Rigaku SmarktLab 9kW), HADDF-STEM (JEOL JEM-ARM200F), TEM (Jeol JEM-2100F) at room temperature or low temperature (with gatan model 636 cooling holder).

Device Fabrication and Electrical Measurement. VSe_2 crystals were first transferred onto SiO_2/Si substrate with 285 nm oxidation layer by pressing the as-grown samples on it. The Hall devices were fabricated by e-beam lithography first and then deposited with 5 nm Ti and 50 nm Au by e-beam evaporation. Magnetotransport measurements were performed by a physical property measurement system (Quantum Design) with magnetic field up to 15 T and temperature from 300 to 2 K.

ACKNOWLEDGMENTS

This work was financially supported by the Hong Kong Polytechnic University grants (1-ZVGH, G-UAEZ, G-YBFT, and G-YBVF), the Research Grants Council of Hong Kong (Project nos. PolyU 153271/16P and PolyU 153039/17P).

ASSOCIATED CONTENT

Supporting Information

This material is available free of charge *via* the Internet.

SEM images, EDS profile, Raman spectroscopy as a function of thickness, AFM height profiles, temperature-dependence of electrical conductivity measurements, temperature dependence of the resistance measurements, and thickness dependence of MR measurements.

AUTHOR INFORMATION

Corresponding Author

*E-mail: apsplau@polyu.edu.hk

Notes

The authors declare no competing financial interest.

REFERENCES

[1] Xi X X, Wang Z F, Zhao W W, Park J –H, Law K T, Berger H, Forró L, Shan J and Mak K F 2016 Ising pairing in superconducting $NbSe_2$ atomic layers *Nat. Phys.* 12 139-143.

[2] Joe Y I, Chen X M, Ghaemi P, Finkelstein K D, de La Peña G A, Gan Y, Lee J C T, Yuan S, Geck J, MacDougall G J, Chiang T C, Cooper S L, Fradkin E and Abbamonte P 2014 Emergence of charge density wave domain walls above the superconducting dome in 1*T*-$TiSe_2$ *Nat. Phys.* 10 421-425.

[3] Wang H X, Huang W, Lin J H, Cui J, Chen Y, Zhu C, Liu F C, Zeng Q S, Zhou J D, Yu P, Wang X W, He H Y, Tsang S H, Gao W B, Suenaga K Z, Ma F C, Yang C L, Lu L, Yu T, Teo E H T, Liu G T and Liu Z 2017 High-quality monolayer superconductor $NbSe_2$ grown by chemical vapour deposition *Nat. Commun.* 8 394-8.

[4] Navarro-Moratalla E, Island J O, Mañas-Valero S, Pinilla-Cienfuegos E, Castellanos-Gomez A, Quereda J, Rubio-Bollinger G, Chirolli L, Silva-Guillén J A, Agraït N, Steele G A, Guinea F, van der Zant H S J and Coronado E 2016 Enhanced superconductivity in atomically thin TaS_2 *Nat. Commun.* 7 11043-7.

[5] Ang R, Tanaka Y, Ieki E, Nakayama K, Sato T, Li L J, Lu W J, Sun Y P and Takahashi T 2012 Real-space coexistence of the melted Mott state and superconductivity in Fe-substituted 1T−TaS_2 *Phys. Rev. Lett.* 109 176403-5.

[6] Ma Y, Dai Y, Guo M, Niu C, Zhu Y and Huang B 2012 Evidence of the existence of magnetism in pristine VX_2 monolayers (X = S, Se) and their strain-induced tunable magnetic properties *ACS Nano* 6 1695.

[7] Zhu X J, Guo Y Q, Cheng H, Dai J, An X D, Zhao J Y, Tian K Z, Wei S Q, Zeng X C, Wu C Z and Xie Y 2016 Signature of coexistence of superconductivity and ferromagnetism in two-dimensional $NbSe_2$ triggered by surface molecular adsorption

Nat. Commun. 7 11210-8.

[8] Xu K, Chen P, Li X, Wu C, Guo Y, Zhao J, Wu X and Xie Y 2013 Ultrathin nanosheets of vanadium diselenide: a metallic two-dimensional material with ferromagnetic charge-density-wave behavior *Angew. Chem., Int. Ed.* 52 10477-10481.

[9] Zhuang H L and Hennig R G **2016** Stability and magnetism of strongly correlated single-layer VS_2 *Phys. Rev. B: Condens.* 93 054429-7.

[10] Bonilla M, Kolekar S, Ma Y, Diaz H C, Kalappattil V, Das R, Eggers T, Gutierrez H R, Phan M H and Batzill M 2018 Strong room-temperature ferromagnetism in VSe_2 monolayers on van der Waals substrates *Nat. Nanotechnol.* 13 289-293.

[11] Xi X, Zhao L, Wang Z, Berger H, Forró L, Shan J and Mak K F 2015 Strongly enhanced charge-density-wave order in monolayer $NbSe_2$ *Nat. Nanotechnol.* 10 765-770.

[12] Kolekar S, Bonilla M, Ma Y, Coy Diaz H and Batzill M 2017 Layer- and substrate-dependent charge density wave criticality in 1T–$TiSe_2$ *2D Mater.* 5 015006-8.

[13] Yang J, Wang W, Liu Y, Du H, Ning W, Zheng G, Jin C, Han Y, Wang N, Yang Z, Tian M and Zhang Y 2014 Thickness dependence of the charge-density-wave transition temperature in VSe_2 *Appl. Phys. Lett.* 105 063109-4.

[14] Terashima K, Sato T, Komatsu H, Takahashi T, Maeda N and Hayashi K 2003 Charge-density wave transition of 1T-VSe_2 studied by angle-resolved photoemission spectroscopy *Phys. Rev. B* 68 155108.

[15] Fu W, Chen Y, Lin J, Wang X, Zeng Q, Zhou J, Zheng L, Wang H, He Y, He H, Fu Q, Suenaga K, Yu T and Liu Z 2016 Controlled synthesis of atomically thin 1T-TaS_2 for tunable charge density wave phase transitions *Chem. Mater.* 28 7613-7618.

[16] Zhang Z, Niu J, Yang P, Gong Y, Ji Q, Shi J, Fang Q, Jiang S, Li H, Zhou X, Gu L, Wu X and Zhang Y 2017 Van der Waals epitaxial growth of 2D metallic vanadium

diselenide single crystals and their extra-high electrical conductivity *Adv. Mater.* 29 1702359-9.

[17] Goli P, Khan J, Wickramaratne D, Lake R K and Balandin A A 2012 Charge density waves in exfoliated films of van der Waals materials: evolution of Raman spectrum in $TiSe_2$ *Nano Lett.* 12 5941-5945.

[18] Zhu X, Cao Y, Zhang J, Plummer E W and Guo Jiandong 2015 Classification of charge density waves based on their nature *Proc. Natl Acad. Sci.* 112 2367-2371.

[19] Weber F, Rosenkranz S, Castellan J –P, Osborn R, Hott R, Heid R, Bohnen K –P, Egami T, Said A H and Reznik D 2011 Extended phonon collapse and the origin of the charge-density wave in 2H-$NbSe_2$ *Phys. Rev. Lett. 107* 107403.

[20] Soumyanarayanan A, Yee M M, He Y, Wezel J, Rahn D J, Rossnagel K, Hudson E W, Norman M R and Hoffman J E **2013** Quantum phase transition from triangular to stripe charge order in $NbSe_2$ *Proc. Natl. Acad. Sci.*110 1623–1627.

[21] Ugeda Miguel M, Bradley Aaron J, Zhang Y, Onishi S, Chen Y, Ruan W, Ojeda-Aristizabal C, Ryu H, Edmonds Mark T, Tsai H –Z, Riss A, Mo S –K, Lee D, Zett A, Hussain Z, Shen Z –X and Crommie Michael F 2016 Characterization of collective ground states in single-layer $NbSe_2$ *Nat. Phy.* 12 92-97.

[22] Kiss T,Yokoya T, Chainani A, Shin S, Hanaguri T, Nohara M and Takagi H **2007** Charge-order-maximized momentum-dependent superconductivity *Nature Phys.* 3 720–725.

[23] Arguello C J, Chockalingam S P, Rosenthal E P, Zhao L, Gutierrez C, Kang J H, Chung W C, Fernandes R M, Jia S, Millis A J, Cava R J and Pasupathy A N 2014 Visualizing the charge density wave transition in 2H-$NbSe_2$ in real space *Phys. Rev. B* 89 235115.

[24] Zhang D, Ha J, Baek H, Chan Y –H, Natterer F D, Myers A F, Schumacher J D,

Cullen W G, Davydov A V, Kuk Y, Chou M Y, Zhitenev N B and Stroscio J A 2017 Strain engineering a 4a×√3a charge-density-wave phase in transition-metaldichalcogenide 1T-VSe_2 *Phys. Rev. Materials* 1 024005-10.

[25] Strocov V N, Shi M, Kobayashi M, Monney C, Wang X, Krempasky J, Schmitt T, Patthey L, Berger H and Blaha P 2012 Three-dimensional electron realm in VSe_2 by soft-x-ray photoelectron spectroscopy: origin of charge-density waves *Phys. Rev. Lett.* 109 086401-5.

[26] Pásztor Á, Scarfato A, Barreteau C, Giannini E and Renner C 2017 Dimensional crossover of the charge density wave transition in thin exfoliated VSe_2 *2D Mater.* 4 041005-6.

[27] Ali M N, Xiong J, Flynn S, Tao J, Gibson Q D, Schoop L M, Liang T, Haldolaarachchige N, Hirschberger M, Ong N P and Cava R J 2014 Large, non-saturating magnetoresistance in WTe_2 *Nature* 514 205-208.

[28] Wang L, Lezama I G, Barreteau C, Ubrig N, Giannini E and Morpurgo A F **2015** Tuning magnetotransport in a compensated semimetal at the atomic scale *Nat. Commun.* 6 8892-7.

[29] Bergmann G 1983 Physical interpretation of weak localization: A time-of-flight experiment with conduction electrons *Phys. Rev. B* 28 2914-2920.

[30] Hongtao L, Lihong B, Zhang Z, Bingyu C, Ruizi Z, Ce B, Ruisong M, Liangmei W, Haifang Y, Junjie L, Changzhi G, Cheng-Min S, Shixuan D, Hong-Jun G 2019 Quasi-2D Transport and Weak Antilocalization E*ff*ect in Few-layered VSe2 *Nano Lett.* 19 4554-4559.

[31] Zheng B, Chen Y, Wang Z, Qi F, Huang Z, Hao X, Li P, Zhang W and Li Y 2016 Vertically oriented few-layered HfS_2 nanosheets: growth mechanism and optical properties *2D Mater*. 3 035024.

[32] Ji Q, Li C, Wang J, Niu J, Gong Y, Zhang Z, Fang Q, Zhang Y, Shi J, Liao L, Wu X, Gu L, Liu Z and Zhang Y 2017 Metallic vanadium disulfide nanosheets as a platform material for multifunctional electrode applications *Nano Lett.* 17 4908-4916.

[33] Chen P, Pai W W, Chan Y –H, Madhavan V, Chou M Y, Mo S –K, Fedorov A –V and Chiang T –C 2018 Unique gap structure and symmetry of the charge density wave in single-layer VSe_2 *Phys. Rev. Lett.*121 196402.

[34] Terashima K, Sato T, Komatsu H and Takahashi T **2003** Charge-density wave transition of 1T-VSe_2 studied by angle-resolved photoemission spectroscopy *Phys. Rev. B* 68 155108.

[35] Wang Z H, Yang L, Li X J, Zhao X T, Wang H L, Zhang Z D and Gao X P A 2014 Granularity controlled nonsaturating linear magnetoresistance in topological insulator Bi_2Te_3 films *Nano Lett*. 14 6510-6514.

[36] Zhang S X, McDonald R D, Shekhter A, Bprii Z X, Li Y, Jia Q X and Picraux S T 2012 Magneto-resistance up to 60 Tesla in topological insulator Bi_2Te_3 thin films *Appl. Phys. Lett*. 101 202403-4.

[37] Xu R, Husmann A, Rosenbaum T F, Saboungi M L, Enderbya J E and Littlewood P B 1997 Large magnetoresistance in non-magnetic silver chalcogenides *Nature* 390 57-60.

[38] Abrikosov A A 1998 Quantum magnetoresistance *Phys. Rev. B* 58 2788-2794.

[39] Cao Q, Yun F F, Sang L, Xiang F, Liu G and Wang X 2017 Defect introduced paramagnetism and weak localization in two-dimensional metal VSe_2 *Nanotechnology* 28 475703.

[40] Barua S, Hatnean M C, Lees M R and Balakrishnan G 2017 Signatures of the Kondo effect in VSe_2 *Sci. Rep.* 7 10964.

[41] Wang H, Chan C H, Suen C H, Lau S P and Dai J –Y 2019 Magnetotransport

properties of layered topological material $ZrTe_2$ thin film *ACS Nano* 13 6008-6016.

[42] Sato T, Terashima K, Souma S, Matsui H, Takahashi T, Yang H, Wang S, Ding H, Maeda N and Hayashi K 2004 Three-dimensional Fermi-surface nesting in 1*T*-VSe_2 studied by angle-resolved photoemission spectroscopy *J. Phys. Soc. Jpn.* 73 3331-3334.

[43] Kolincio K K, Roman M and Klimczuk T 2019 Charge density wave and large nonsaturating magnetoresistance in $YNiC_2$ and $LuNiC_2$ *Phys. Rev. B 99* 205127.

[44] Neal AT, Du Y, Liu H and Ye P D 2014 Two-dimensional $TaSe_2$ metallic crystals: spin orbit scattering length and breakdown current density *ACS Nano* 8 9137-9142.

[45] Lin J J and Bird J P 2002 Recent experimental studies of electron dephasing in metal and semiconductor mesoscopic structures *J. Phys.-Condes. Matter* 14 R501-R596.

[46] Du Y, Neal A T, Zhou H and Ye P D 2016 Transport studies in 2D transition metal dichalcogenides and black phosphorus *J. Phys.-Condes. Matter* 28 263002-13.

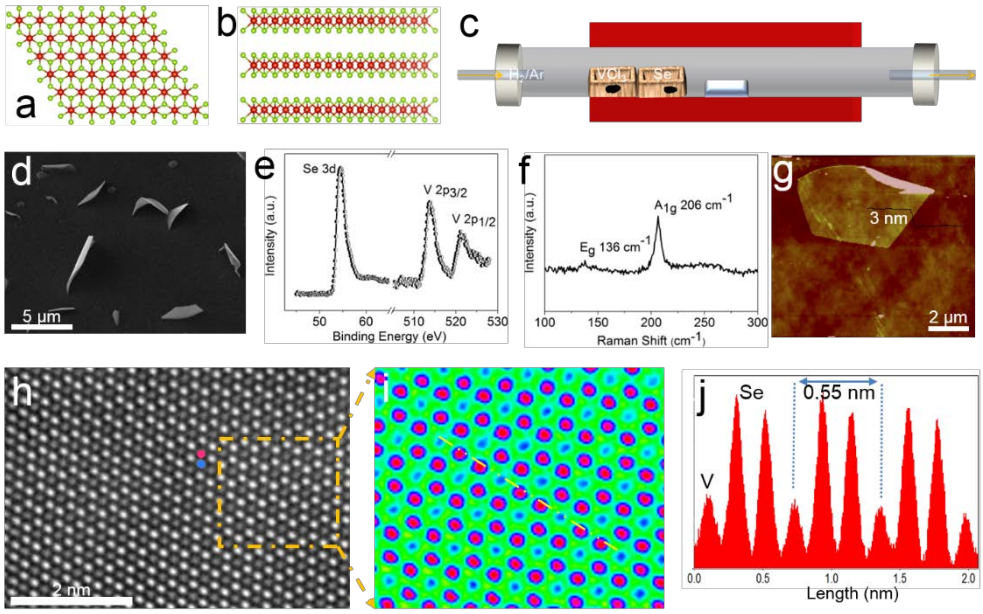

Figure 1. CVD growth and characterizations of VSe_2 crystals. (a and b) 3D schematic model of VSe_2 viewed form top (a) and side (b), red and green balls represent V and Se, respectively. (c) Schematic illustration of the CVD growth VSe_2 route. (d) SEM image reveals the standing VSe_2 crystals on the sapphire substrate. (e) XPS spectrum of V 2p and Se 3d for VSe_2 on Si substrate. (f) Raman spectrum of the as-grown VSe_2 on sapphire substrate. (g) AFM image and corresponding height profile of VSe_2 crystal with 3 nm thick. (h) Atomic resolution HAADF-STEM image of the VSe_2, gray and white balls which are marked with blue and red circle represent V and Se atoms, respectively. (i) Zoom in image of the area marked with a dashed yellow rectangle in (h), with the false color coded according to HAADF intensity. The V and Se atoms are colored with blue and red, respectively. (j) Intensity profile along the dashed yellow line in (d).

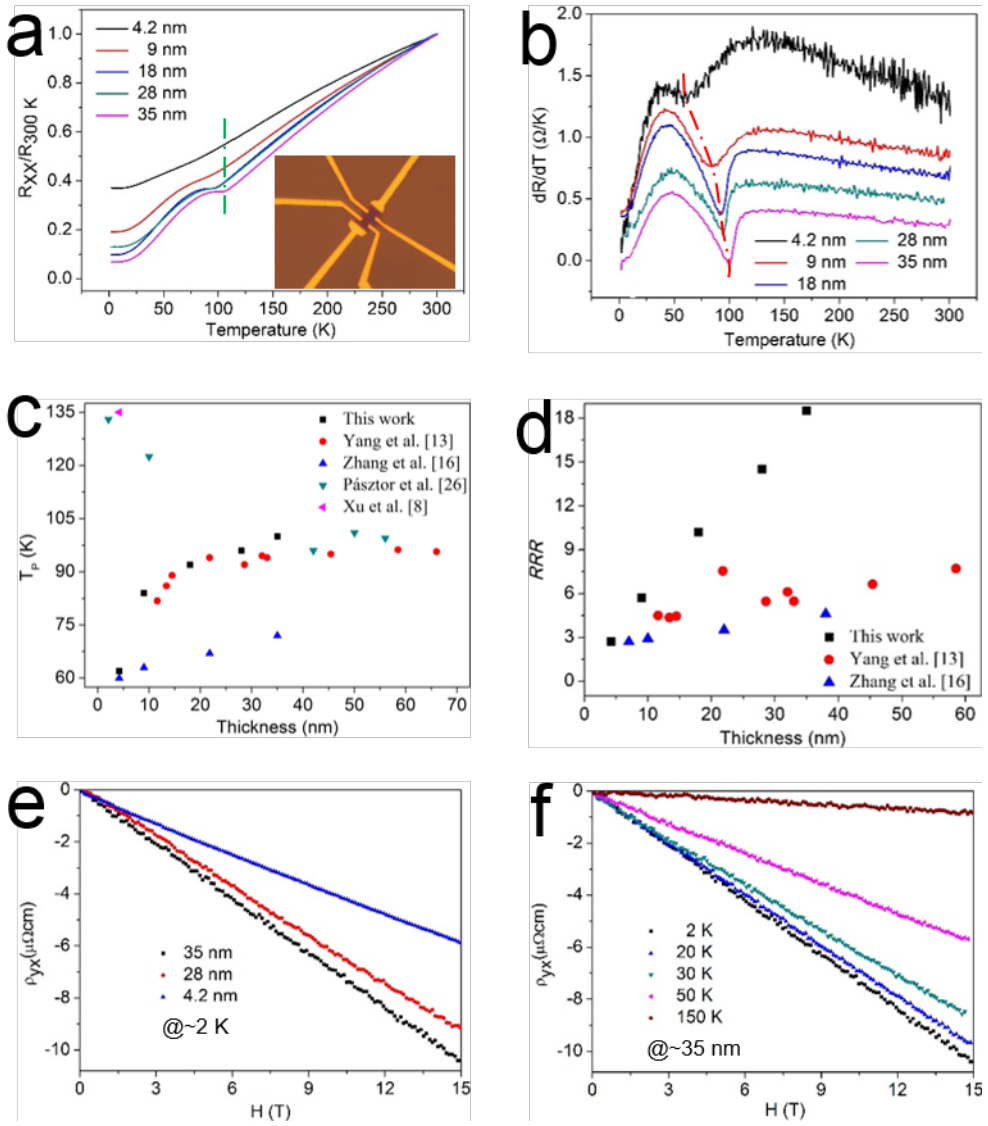

Figure 2. (a) Temperature dependent resistivity of VSe_2 crystals as a function of thickness, the inset in (a) is the optical microscope image of a six-terminal Hall bar device on SiO_2/Si substrate. (b) First derivative of the resistivity of VSe_2 crystals with thicknesses corresponding to (a). The red dashed line indicates the minima of dR/dT at different thicknesses. (c) Comparison of the CDW T_p with the literature. (d) Comparison of RRR values among different works for VSe_2 nanosheets. (e) Magnetic field dependence of Hall resistivity ρ_{xy} for VSe_2 crystals with different thicknesses at 2 K. (f) Magnetic field dependence of Hall resistivity ρ_{xy} for the 35-nm-thick VSe_2 crystal at selected temperatures.

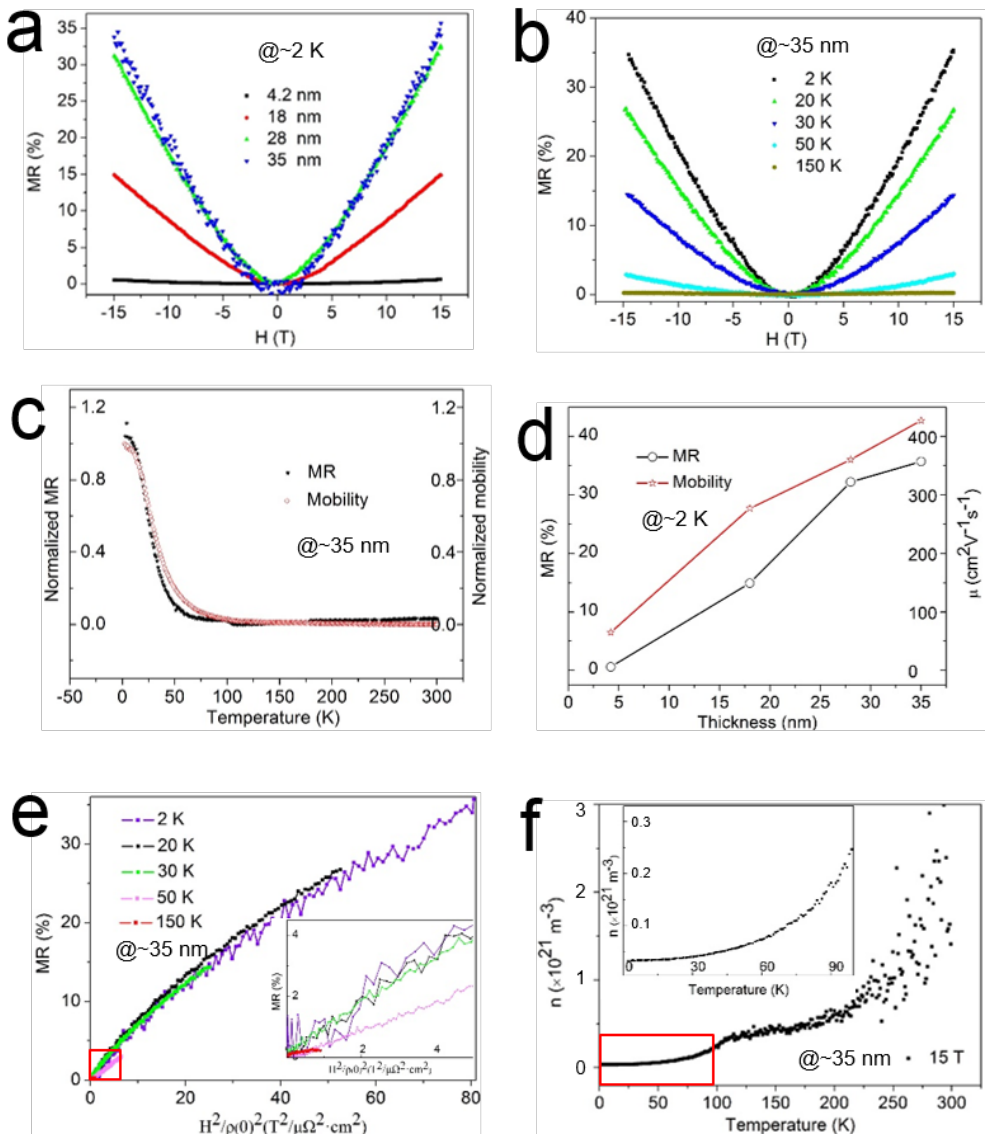

Figure 3. (a) Magnetic field dependence of MR for VSe_2 crystals with various thicknesses at 2 K. (b) Magnetic field dependence of MR for 35-nm-thick VSe_2 at different temperatures. (c) Temperature dependence of MR and mobility. (d) Thickness dependence of MR and mobility, indicating the consistent trends of MR and the mobilities of the VSe_2 as a function of temperature. (e) Kohler's plots of the 35-nm-thick VSe_2 at various denoted temperatures. The inset is the enlargement of red boxed region. (f) Temperature dependence of carrier density. The inset is the enlargement of red boxed region.

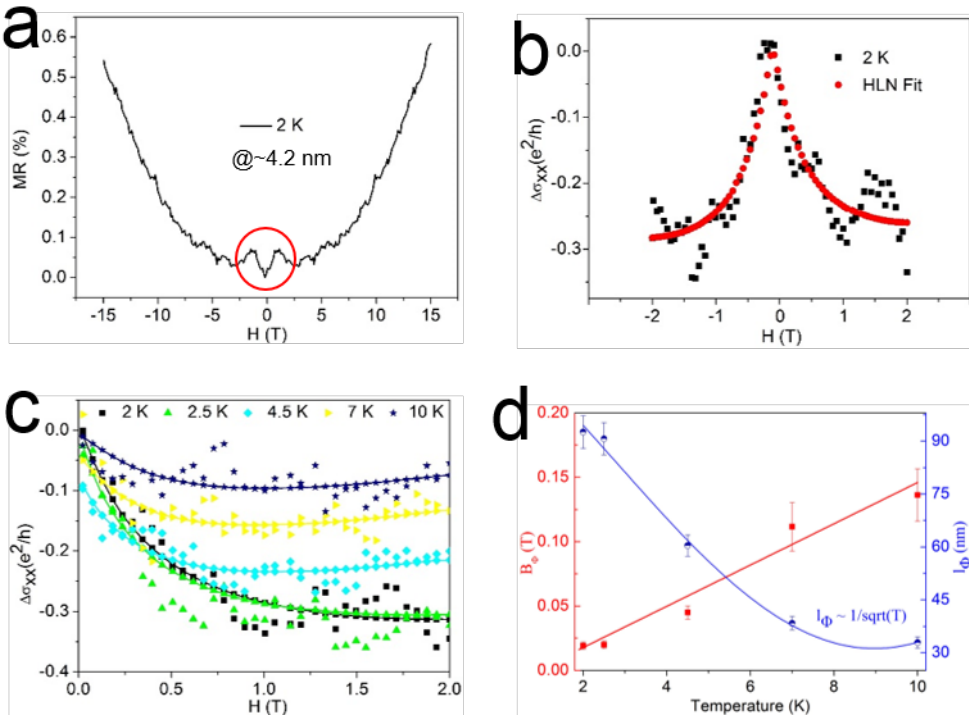

Figure 4. (a) Magnetic field dependence of MR for the 4.2-nm-thick VSe_2, a sharp dip can be observed at the low magnetic fields signaling the WAL effect. (b) The enlarged region of the red circle in (a) with the fitting result by HLN formula. (c) Magnetic field dependence of the magnetoconductance with the HLN fitting results at different temperatures. The dashed symbols are the experiment data and the solid lines are the fitting curves. (d) Temperature dependence of dephasing field $B_{\emptyset}$ and phase coherence length $l_{\emptyset}$, extracted from the HLN fittings of the 4.2-nm-thick VSe_2.

The table of contents entry

Low temperature transport study of high-quality ultrathin VSe_2 single crystals demonstrates that the non-applicability of Kohler's rule, abrupt changes in conductivity and carrier mobility indicate the charge-density-wave (CDW) pseudo gap opening in the Fermi surface. The ultrathin (4.2-nm-thick) VSe_2 demonstrates weak antilocalization effect at low field. These results open new avenues to study the fundamental quantum phenomena in CVD-deposited TMDs.

Title: Thickness-Dependent Magnetotransport Properties in 1T VSe_2 Single Crystals Prepared by Chemical Vapor Deposition

Keywords: Vanadium Diselenide, Chemical Vapor Deposition, Charge Density Wave, Magnetoresistance, Weak Antilocalization

TOC figure: